NACA

RESEARCH MEMORANDUM

PERFORMANCE CHARACTERISTICS OF AXISYMMETRIC TWO-CONE AND ISENTROPIC NOSE INLETS AT MACH NUMBER 1.90

By James F. Connors and Rudolph C. Meyer

Lewis Flight Propulsion Laboratory
Cleveland, Ohio

NATIONAL ADVISORY COMMITTEE
FOR AERONAUTICS

WASHINGTON

December 7, 1955
Declassified September 1, 1959

N

NATIONAL ADVISORY COMMITTEE FOR AERONAUTICS

RESEARCH MEMORANDUM

PERFORMANCE CHARACTERISTICS OF AXISYMMETRIC TWO-CONE AND ISENTROPIC NOSE INLETS AT MACH NUMBER 1.90

By James F. Connors and Rudolph C. Meyer

3706

SUMMARY

An experimental investigation was conducted at a Mach number of 1.90 to determine the over-all performance capabilities of axisymmetric two-cone and isentropic nose inlets in terms of total-pressure recovery, mass flow, and external drags. At zero angle of attack, the external drags were separated into their components of cowl pressure, friction, and additive drags. For angles of attack up to 8°, only internal-flow performance was determined.

At zero angle of attack, critical total-pressure recoveries of 0.94 and 0.92 were obtained with the isentropic inlet and with the two-cone inlet, respectively. With an alternate cowl which had an initially rapid area expansion, the two-cone inlet also realized a total-pressure recovery of 0.94. Each inlet captured essentially the maximum stream-tube of air. At zero angle of attack, stable subcritical operating ranges of approximately 30 percent of maximum mass flow were obtained. With suction on the first cone of the two-cone inlet, the range of stable subcritical operation was increased to 90 percent of maximum mass flow.

The isentropic inlet had a cowl-pressure drag coefficient (0.155 based on maximum frontal area) which was 29 percent larger than that for the two-cone inlet (0.12). In a thrust-minus-nacelle-drag comparison based on a typical turbojet application with afterburning, the isentropic inlet was marginally better (0.6 percent) than the two-cone inlet and approximately 3 percent better than a representative high-recovery one-cone inlet.

For angles of attack greater than 5°, the pressure recovery and mass-flow performance of the two-cone inlet was superior to that of the isentropic inlet.

INTRODUCTION

In the Mach number range of 2.0, most nacelle-inlet investigations dealing with combined pressure recovery and drag evaluations have been concerned primarily with the single-cone geometries. This type of inlet is capable of achieving kinetic-energy efficiencies up to 95 percent with small to moderate cowl drags. For current turbojet engines, the attainment of correspondingly higher total-pressure recoveries can increase both the altitude limits and the thrust margins for acceleration. There is then a need for further study and evaluation of the higher compression inlets wherein pressure recovery and cowl drag are weighed in terms of over-all power-plant performance.

3706

The present investigation was conducted to determine the capabilities of axisymmetric inlets designed for near maximum pressure recovery with maximum capture mass flow. Specifically, the experimental configurations consisted of a two-cone and an isentropic inlet. In addition to the design geometries, the two-cone inlet was investigated with boundary-layer suction on the initial cone and with an alternate cowl producing an initially rapid area divergence. The isentropic inlet was studied with and without a constant-effective-area throat length. At zero angle of attack, the external drag was separated into its components of cowl-pressure, additive, and friction drags. For angles of attack up to 8°, only internal-flow performance was determined.

SYMBOLS

The following symbols are used in this report:

A_e	minimum flow area at entrance to diffuser (throat), sq ft
A_i	cowl capture area defined by cowl-lip diameter, sq ft
A_{max}	maximum frontal area of model, 0.1364 sq ft
C_D	drag coefficient, $\frac{D}{q_0 A_{max}}$
$C_{D,a}$	additive drag coefficient, $\frac{D_{additive}}{q_0 A_{max}}$
$C_{D,c}$	cowl-pressure drag coefficient, $\frac{D_{cowl\text{-}pressure}}{q_0 A_{max}}$
$C_{D,c,i}$	cowl-pressure drag coefficient based on A_i, $\frac{D_{cowl\text{-}pressure}}{q_0 A_i}$
C_p	pressure coefficient

D drag, lb

D_c cowl-pressure drag, lb

F thrust, lb

F_i ideal thrust based on 100 percent recovery, lb

M local Mach number

3706

M_e average Mach number at entrance to diffuser

M_0 free-stream Mach number

m_B mass-flow bled-off through suction holes, slugs/sec

m_0 maximum possible capture mass flow $(\rho_0 V_0 A_i)$, slugs/sec

m_3 mass flow passing through diffuser exit, slugs/sec

P_0 free-stream total pressure, lb/sq ft

P_3 total pressure at diffuser exit, lb/sq ft

p_0 free-stream static pressure, lb/sq ft

q_0 free-stream dynamic pressure, $\frac{\gamma}{2} p_0 M_0^2$, lb/sq ft

V_0 free-stream velocity, ft/sec

α angle of attack, deg

γ ratio of specific heats for air, 1.4

θ flow angle with respect to horizontal axis, deg

ρ_0 free-stream density, slugs/cu ft

APPARATUS AND PROCEDURE

The experimental program was conducted at a Mach number of 1.90 in the NACA Lewis 18- by 18-inch supersonic wind tunnel. In the test chamber, the air was maintained at a stagnation temperature of 150±5° F and at a dew-point temperature of -25±5° F. The simulated pressure altitude was approximately 45,000 feet. The Reynolds number based on the maximum diameter of the model (5 in.) was 1.33×10^6.

As illustrated in the cut-away drawing of figure 1(a), the 5-inch-diameter model was sting-mounted off the main tunnel support strut. An adjustable exit-plug was provided for regulating the inlet back pressure and was mounted independent of the three-component balance system. On the front end of the model, provisions were incorporated for interchangeable spikes and cowls.

A photograph of the experimental spikes and cowls of the two-cone and isentropic inlets is shown in figure 1(b), and their coordinate dimensions are listed in table I. Pertinent aerodynamic design details are indicated in the sketches of figure 1(c). The two-cone inlet had a 20° initial half-cone angle and a 28° second half-cone angle, which represented a near optimum combination of angles from a theoretical recovery standpoint. In order to locate the oblique shock intersection and thus the cowl-lip position, a curved second shock was calculated by assuming a constant flow deflection (8°) across the conical field of the first cone. The isentropic spike had an initial 20° half-cone angle followed by an isentropic compression surface designed by the method of characteristics with the specification of point turning (focused compression) at the cowl lip. With both inlets the compression was carried down to a final Mach number M_e of approximately 1.26 at the diffuser entrance. The theoretical total-pressure recovery based solely on shock losses was approximately 0.97 for each inlet.

The internal cowl surfaces for both inlets were alined initially in the local stream direction, and the external cowl-lip angles were slightly less than the value for shock detachment at free-stream Mach number. Approximately constant-area turning of the flow back to the axial direction was employed. The rate of flow turning, in both cases, was largely dictated by the necessity of holding the internal surface Mach number along the cowl (~ 1.3) nearly constant until the expansion waves from the spike shoulder cancelled any further compressive turning. This procedure avoided local shock detachment along the internal cowl surface.

The flow-area distribution in the internal ducting is shown in figure 1(d). Neither inlet was designed for internal contraction. The two-cone inlet had an initial 3-hydraulic-diameter length of approximately constant effective flow area; while, the isentropic inlet had two versions, one with and one without the constant-effective-area section. The purpose of these sections was to determine the effect upon subcritical flow stabilization as demonstrated in reference 1. The two-cone (alternate cowl) inlet was actually a combination of the two-cone spike and the cowl of the isentropic inlet. As illustrated in figure 1(d), the resulting area distribution showed an initially rapid area divergence (approximately an equivalent 10°-included-angle conical-area expansion) followed by a slight contraction back to the point which is common to all configurations. Downstream of the common joint, the area distribution of the subsonic diffuser conformed approximately to that of an equivalent 5°-included-angle conical-area expansion.

The application of suction on the initial cone surface of the two-cone inlet was investigated in order to determine its effectiveness in extending the subcritical stability range. This was accomplished by drilling two double rows of holes on the spike, as shown in figure 1(e), and venting the centerbody to free-stream static pressure. Two additional hollow struts were used to provide a passage for this bleed flow to the free stream. Each strut had a 3-inch chord and was 1/2 inch thick with a round leading edge located at an axial station $2\frac{1}{2}$ inches downstream of the cowl lip.

3706

Pressure instrumentation consisted of a 24-tube total-pressure rake and four wall static-pressure taps at the diffuser exit, three static taps (90° apart) on the base, one static tap in the balance chamber, and 29 static taps on the inlet cowls. Total-pressure recovery was based on an area-weighted integration of the rake pressures. Mass flow was computed from the static pressure at the rake station and the sonic discharge area with the assumption of isentropic one-dimensional flow. At zero angle of attack, the mass-flow measuring technique was checked by testing an inlet (two-cone inlet with a 1/16-in. cowl spacer) that captured a known free streamtube of air. Integrating the static-pressure distribution determined cowl-pressure drag. In order to obtain the total drag, the internal thrust (total momentum at rake minus inlet total momentum) and the base force were subtracted from the balance force. External friction drag was evaluated by subtracting the cowl-pressure drag from the total drag for an inlet capturing a full free streamtube of air (zero additive drag). This value was checked for order of magnitude at critical mass flow by a momentum integration of the external-skin boundary-layer profile as determined from experimental probe surveys at the base of the model. No force data were taken at angle of attack because of shock reflections from the tunnel walls.

RESULTS AND DISCUSSION

Total-Pressure Recovery and Mass-Flow Characteristics

The diffuser performance characteristics of the various inlet configurations are presented in figure 2. At zero angle of attack, the two-cone inlet (fig. 2(a)) gave a maximum total-pressure recovery of 0.92 with a corresponding maximum mass-flow ratio of 0.995. Stable subcritical operation was obtained down to a mass-flow ratio of 0.70 and a corresponding pressure recovery of 0.85. As shown in figure 2(b), the isentropic inlet yielded a pressure recovery of 0.94 at a mass-flow ratio of 0.995 and was stable subcritically down to a mass-flow ratio of 0.67.

Also at zero angle of attack, the two-cone (alternate cowl) inlet, a combination of the two-cone spike and the isentropic cowl, indicated an internal-flow performance (fig. 2(c)) quite similar to that of the isentropic inlet. The reason for the improved performance of this inlet in comparison with that of the original two-cone inlet is not fully understood in view of what was first considered its poor internal-duct area variation (fig. 1(d)). However, similar observations have been made with other inlet configurations. For example, reference 2 suggests that such improvement resulted from a reduction in subsonic frictional losses effected by the initially rapid lowering of the subsonic entrance Mach number. It may also be that in the present case the slight (1°) flow expansion at the cowl lip caused an improved orientation of the diffuser shock during critical operation by minimizing the effects of shock-boundary-layer interaction at the cowl by means of a favorable pressure gradient.

3706

Adding 3 hydraulic diameters of constant effective-flow-area length to the isentropic inlet (fig. 2(d)) produced no favorable effects on performance with regard either to pressure recovery or subcritical stability range.

Schlieren photographs of the inlet air-flow patterns are presented in figure 3. At zero angle of attack, with both the two-cone and the isentropic inlets, the oblique shocks during supercritical operation appeared to fall very close to or even inside the cowl lip. As the normal shock moved out ahead of the cowl, the slipline or vortex sheet from the shock intersection moved in toward the spike and away from the cowl, as prescribed in reference 3 for stable regulation of subcritical flow. In the intermediate subcritical shock positions, the bow shock stood on the centerbody compression surface without producing any apparent separation of the boundary layer. Downstream of the shock - boundary-layer interaction zone, the boundary layer seemed to be attached and to follow the spike contour back into the inlet. This was in accordance with reference 4, which suggests that a static-pressure rise of 1.89 is required for separation of a turbulent layer. For the present case, the pressure rise across the diffuser normal shock as it first moved out on the spike was only 1.5. The minimum stable mass-flow condition was attained when the bow shock was positioned at the break between the conical surfaces of the two-cone inlet and at a comparable location for the isentropic inlet. As a probable consequence of increased shock strength (due to higher surface Mach numbers), any attempt to position the bow wave farther upstream on the spike would initiate a pulsing flow or inlet buzz. At the onset of buzz, the boundary layer quite definitely appeared to lift and separate from the surface. This separation apparently initiated and maintained the buzz cycle in the sense of an alternate choking and unchoking of the duct flow (see ref. 5).

In order to extend the stable subcritical range, an attempt to control the boundary layer on the first cone of the two-cone inlet was made by applying surface suction through several rows of bleed holes. The results are shown in figure 2(e). An additional pair of struts (as described in APPARATUS) was necessary for venting the centerbody. These struts forced a supercritical bow shock to stand ahead of the cowl with a resultant decrease in maximum mass-flow ratio of 11 percent and a reduced critical pressure recovery. However, without suction the minimum stable mass-flow condition was, for all purposes, the same with or without the hollow struts with respect to shock position, pressure recovery, and mass flow. Thus, it is felt that any effects of suction in extending the stable subcritical range would not be compromised by the struts, and the results would be equally applicable to the design configuration with another bleed arrangement that would allow for full-capture mass flow (no supercritical spillage). As shown by the data in figure 2(e), with two rows of bleed holes just upstream of the break between the two cones, subcritical stability was extended down to a mass-flow ratio of 0.52. With a total of four rows of holes and an estimated bleed mass-flow ratio m_B/m_0 of 0.015, stable operation was obtained down to a mass-flow ratio m_3/m_0 of 0.12. For minimum stable m_3/m_0 with no suction to minimum stable m_3/m_0 with full suction, the total-pressure recovery decreased only slightly from 0.85 to 0.81.

In figure 3(c) the corresponding flow patterns obtained for the two-cone inlet with suction applied on the first cone are shown. Supercritically, a bow shock was located ahead of the cowl lip. With full suction, minimum stable operation ($m_3/m_0 \sim 0.1$) occurred with the bow shock appearing, by extrapolation of the visible shock structure, to stand well upstream of the first row of bleed holes. If such were the case, the effectiveness of suction was maintained for a limited range even after the bow shock passed over the holes and acquired some farther upstream position. Intermediate subcritical operation was quite stable over the entire range of mass flows with the surface boundary layer apparently attached as it entered the inlet. The effects of suction were determined only for zero angle of attack.

The effect of angle of attack on inlet performance is summarized in the cross plot of figure 4. Generally, angle of attack caused reductions in pressure recovery, mass flow, and subcritical stability range. With both the two-cone and isentropic inlets, subcritical stability decreased from approximately 30 percent of maximum mass flow at zero angle of attack to approximately 7 percent at an angle of attack of 8°. The isentropic inlet performance (both pressure recovery and mass flow) fell off more rapidly with increasing angle of attack than that of the two-cone inlet. For angles of attack greater than 5°, the two-cone inlet was superior to the isentropic inlet.

Angle-of-attack air-flow patterns are shown for the two-cone and isentropic inlets in figure 3. With angle of attack, cross-flow effects generally produced a thickening boundary layer on the top or lee side of the compression surfaces, which probably had some effect in reducing the subcritical stability range. Otherwise, angle of attack resulted in increasing spillage in the top quadrant of the inlet and increasingly stronger shocks due to the additional compression in the lower quadrant.

Total-Pressure Profiles at Diffuser Exit

The total-pressure distributions across the diffuser exit are presented for both the two-cone and the isentropic inlets at approximately critical operation in figure 5. These profiles were measured on a rake approximately 3/8 diameter downstream of the actual diffuser exit in a constant-area section. At zero angle of attack, both inlets indicated a somewhat parabolic radial distribution with no appreciable circumferential distortion. For these operating conditions, relatively high average Mach numbers occurred at the rake station ($M_3 \sim 0.42$ with the sting, corresponding to $M_3 \sim 0.34$ without sting). With increasing angle of attack, the total-pressure profiles steepened with an increasing tendency toward flow separation in the lower quadrants of the ducts. The isentropic inlet indicated a slightly more pronounced tendency toward separation at angle of attack when compared with the two-cone inlet.

Cowl-Pressure Distributions and Drag

In figure 6 static-pressure distributions along the cowls are presented for supercritical, subcritical, and minimum stable mass-flow conditions. Also included for comparison are the theoretical distributions for supercritical flow based on a two-dimensional-flow shock-expansion method (ref. 6). Linearized theory in this case is inapplicable because of the large cowl angles. In each case, the theoretical values overestimated the surface pressures. With increasing mass-flow spillage, all the pressure coefficients decreased; negative pressure coefficients in the vicinity of the sharp leading edge of the cowls indicated suction forces at reduced mass flows.

From area-weighted integrations of the static-pressure distributions, cowl-pressure drag coefficients were obtained and are presented as functions of mass-flow ratio in figure 7. The two-dimensional-flow shock-expansion theory for each cowl overestimated the pressure drag coefficient by 15 percent. Because of a greater external lip angle and a larger projected area, the isentropic cowl exhibited a drag ($C_{D,c} = 0.155$) which was 29 percent higher than that for the cowl of the two-cone inlet ($C_{D,c} = 0.12$). As illustrated by the data, cowl-pressure drag decreased linearly with decreasing mass-flow ratio with each cowl having approximately the same slope.

3706

Zero-Angle-of-Attack Component Breakdown of External Drag

External-flow characteristics (i.e., drags) for the two-cone (alternate cowl) inlet were not determined, since they would be identical to those for the isentropic inlet at zero angle of attack. The total external drags and their components of friction, cowl-pressure, and additive drags for the two-cone and the isentropic inlets are presented in figure 8. Friction drags were obtained by subtracting the supercritical cowl-pressure drags ($C_{D,a} = 0$) from the total drags as obtained through balance measurements. Order of magnitude was checked by a momentum integration of the external boundary layer. This friction drag was then assumed constant with mass-flow spillage as in references 7 and 8. Accordingly, additive drag increased rapidly and linearly with reduced mass flow. For a specified flow spillage, the magnitude of the additive drag was approximately the same for both the two-cone and the isentropic inlets. For engineering purposes, it was found that the additive drag of these inlets could be predicted with sufficient accuracy by calculating $C_{D,a}$ for a 60° one-cone inlet. This cone angle approximated the maximum compression surface angles of the two-cone and isentropic inlets. At a mass-flow ratio of 0.7, $C_{D,a}$ was 0.30, as estimated for a 60° cone by the method of reference 9, compared with a $C_{D,a}$ of approximately 0.31 from figure 8 for both the two-cone and the isentropic inlets.

At corresponding mass-flow ratios, the magnitudes of the total external drags for the two-cone inlet (fig. 8(a)) were lower than those for the isentropic inlet (fig. 8(b)) by the difference in cowl-pressure drags.

Over-All Performance Comparison

In order to evaluate the merit of obtaining increased inlet total-pressure recoveries at the expense of a concomitant cowl-drag rise, the two-cone and the isentropic inlets were compared on a propulsive thrust basis with two representative one-cone inlets (refs. 10 and 11). The results for zero angle of attack at a free-stream Mach number of 1.90 are shown in the following table:

Inlet configuration	Total-pressure recovery, P_3/P_0	Cowl-pressure drag coefficient based on A_i, $C_{D,c,i}$	Propulsive thrust ratio, $\frac{F - D_c}{F_i}$
Isentropic	0.94	0.225	0.855
Two-cone	.92	.165	.850
One-cone (ref. 10)	.90	.15	.829
One-Cone (ref. 11)	.84	.065	.780

3706

The reference one-cone inlet data involved some interpolation between Mach numbers. These particular one-cone inlets were selected to indicate the performance levels of typical high-recovery and low-drag configurations. The method of reference 12 was used to compute the ratio of thrust minus cowl-pressure drag to ideal thrust for each inlet installed on a typical turbojet engine with afterburning to 3500° R. The isentropic inlet appeared to be the best on a propulsive-thrust basis. However, the two-cone inlet with its much lower cowl drag was only marginally lower (0.6 percent), and the one-cone inlet of reference 10 was approximately 3 percent lower than the isentropic inlet. The maximum difference in thrust minus nacelle-drag for these particular inlets was approximately 10 percent.

SUMMARY OF RESULTS

An experimental investigation of axisymmetric two-cone and isentropic nose inlets at Mach number 1.90 yielded the following results:

1. A critical total-pressure recovery of 0.94 was obtained with the isentropic inlet and with a two-cone (alternate cowl) inlet that had an initially rapid internal-area expansion. The design two-cone inlet realized a total-pressure recovery of 0.92. Each inlet captured essentially a maximum streamtube of air (i.e., a mass-flow ratio ≈ 1.0).

2. At zero angle of attack, the isentropic and two-cone inlets had stable subcritical operating ranges of approximately 30 percent of maximum mass flow. With the two-cone inlet at zero angle of attack, the stable subcritical operating range was increased to 90 percent of maximum mass flow by means of boundary-layer suction on the initial cone surface. The corresponding maximum bleed mass flow was estimated at

approximately 1.5 percent of the maximum possible mass flow into the inlet.

3. Angle of attack generally reduced pressure recovery, capture mass flow, and subcritical stability range. Because its critical performance (pressure recovery and mass flow) fell off more rapidly with increasing angle of attack, the isentropic inlet became inferior to the two-cone inlet at angles of attack greater than 5°.

3706

4. The isentropic inlet had a cowl-pressure drag coefficient (0.155 based on maximum frontal area) which was 29 percent larger than that for the two-cone inlet (0.12).

5. In a thrust minus nacelle-drag comparison based on a typical turbojet application with afterburning, the isentropic inlet at zero angle of attack was marginally better (0.6 percent) than the two-cone inlet and about 3 percent better than a representative high-recovery one-cone inlet.

Lewis Flight Propulsion Laboratory
National Advisory Committee for Aeronautics
Cleveland, Ohio, July 1, 1955

REFERENCES

1. Nettles, J. C.: The Effect of Initial Rate of Subsonic Diffusion on the Stable Subcritical Mass-Flow Range of a Conical Shock Diffuser. NACA RM E53E26, 1953.

2. Davids, Joseph, and Wise, George A.: Investigation at Mach Numbers 1.5 and 1.7 of Twin-Duct Side Intake System with Two-Dimensional 6° Compression Ramps Mounted on a Supersonic Airplane. NACA RM E53H19, 1953.

3. Ferri, Antonio, and Nucci, Louis M.: The Origin of Aerodynamic Instability of Supersonic Inlets at Subcritical Conditions. NACA RM L50K30, 1951.

4. Nussdorfer, T. J.: Some Observations of Shock-Induced Turbulent Separation on Supersonic Diffusers. NACA RM E51L26, 1954.

5. Dailey, C. L.: Supersonic Diffuser Instability. Doctoral Thesis, GALCIT, 1954.

6. Eggers, A. J., Jr., Savin, R. C., and Syverston, C. A.: The Generalized Shock-Expansion Method and Its Application to Bodies Traveling at High Supersonic Airspeeds. Preprint No. 487, Jour. Inst. Aero. Sci., 1954.

7. Nussdorfer, T., Wilcox, F., and Perchonok, E.: Investigation at Zero Angle of Attack of a 16-Inch Ram-Jet Engine in 8- by 6-Foot Supersonic Wind Tunnel. NACA RM E50L04, 1951.

8. Esenwein, Fred T., and Valerino, Alfred S.: Force and Pressure Characteristics for a Series of Nose Inlets at Mach Numbers from 1.59 to 1.99. I - Conical Spike All-External Compression Inlet with Subsonic Cowl Lip. NACA RM E50J26, 1951.

9. Sibulkin, Merwin: Theoretical and Experimental Investigation of Additive Drag. NACA Rep. 1187, 1954. (Supersedes NACA RM E51B13.)

10. Gorton, Gerald C., and Dryer, Murray: Comparison at Supersonic Speeds of Translating Spike Inlets Having Blunt- and Sharp-Lip Cowls. NACA RM E54J07, 1955.

11. Weinstein, Maynard I., and Davids, Joseph: Force and Pressure Characteristics for a Series of Nose Inlets at Mach Numbers from 1.59 to 1.99. III - Conical-Spike All-External-Compression Inlet with Supersonic Cowl Lip. NACA RM E50J30, 1951.

12. Kremzier, Emil J.: A Method for Evaluating the Effects of Drag and Inlet Pressure Recovery on Propulsion-System Performance. NACA TN 3261, 1954.

3706

3706

TABLE I. - INLET DIMENSIONS

[All cowls have leading-edge radius of 0.0025 in.]

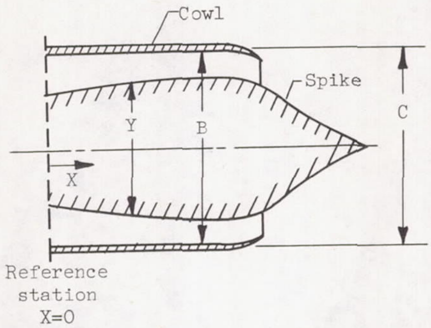

Two-cone inlet					Isentropic inlet					Long isentropic inlet				
Spike		Cowl			Spike		Cowl			Spike		Cowl		
X	Y	X	B	C	X	Y	X	B	C	X	Y	X	B	C
0.129	2.712	0	4.544	5.000	0.129	2.712	0	4.544	5.000	0.129	2.712	0	4.544	5.000
.887	2.780	Straight taper		Cylin-	.879	2.814	.750	4.584	Cylin-	1.629	2.900	.500	4.562	Cylin-
1.887	2.860			drical	1.629	2.938	1.500	4.640	drical	2.379	3.004	1.500	4.602	drical
2.887	2.934	4.500	4.740	5.000	2.379	3.072	2.500	4.706	↓	3.129	3.100	2.500	4.650	↓
3.887	3.006	4.700	4.750	5.000	3.129	3.180	3.500	4.760		3.879	3.164	3.500	4.690	
4.887	3.092	4.900	4.750	5.000	3.879	3.268	4.000	4.780		4.629	3.212	4.500	4.730	
5.087	3.104	5.000	-----	5.000	4.629	3.326	4.500	4.788		5.379	3.250	5.500	4.760	
5.287	3.088	5.200	4.734	-----	5.029	3.330	4.750	4.788		6.129	3.280	6.500	4.780	
5.487	3.012	5.400	-----	4.900	5.229	3.310	5.000	4.780	5.000	6.879	3.308	7.000	4.784	
5.687	2.906	5.600	4.642	-----	5.429	3.256	5.250	4.740	4.942	7.629	3.326	7.500	4.788	
5.887	2.778	5.900	4.528	4.646	5.629	3.156	5.500	4.684	4.846	8.029	3.330	7.750	4.788	5.000
6.087	2.638	6.200	-----	4.458	5.829	3.000	5.700	4.606	4.738	8.229	3.310	8.000	4.780	5.000
7.282	2.470	6.300	4.350	-----	6.029	2.816	5.900	4.494	4.598	8.429	3.256	8.250	4.740	4.942
7.359	1.324	6.500	4.250	4.250	6.229	2.602	6.100	4.382	-----	8.629	3.156	8.500	4.684	4.846
9.187	0	-----	-----	-----	6.629	2.142	6.300	4.266	-----	8.829	3.000	8.700	4.606	4.738
					6.849	1.888	6.500	4.144	-----	9.029	2.816	8.900	4.494	4.598
					7.049	1.662				9.229	2.602	9.100	4.382	-----
					7.249	1.456				9.629	2.142	9.300	4.266	-----
					7.449	1.270				9.849	1.888	9.500	4.144	-----
					7.649	1.102				10.049	1.662			
					7.849	.948				10.249	1.456			
					9.149	0				10.449	1.270			
										10.649	1.102			
										10.849	.948			
										12.149	0			

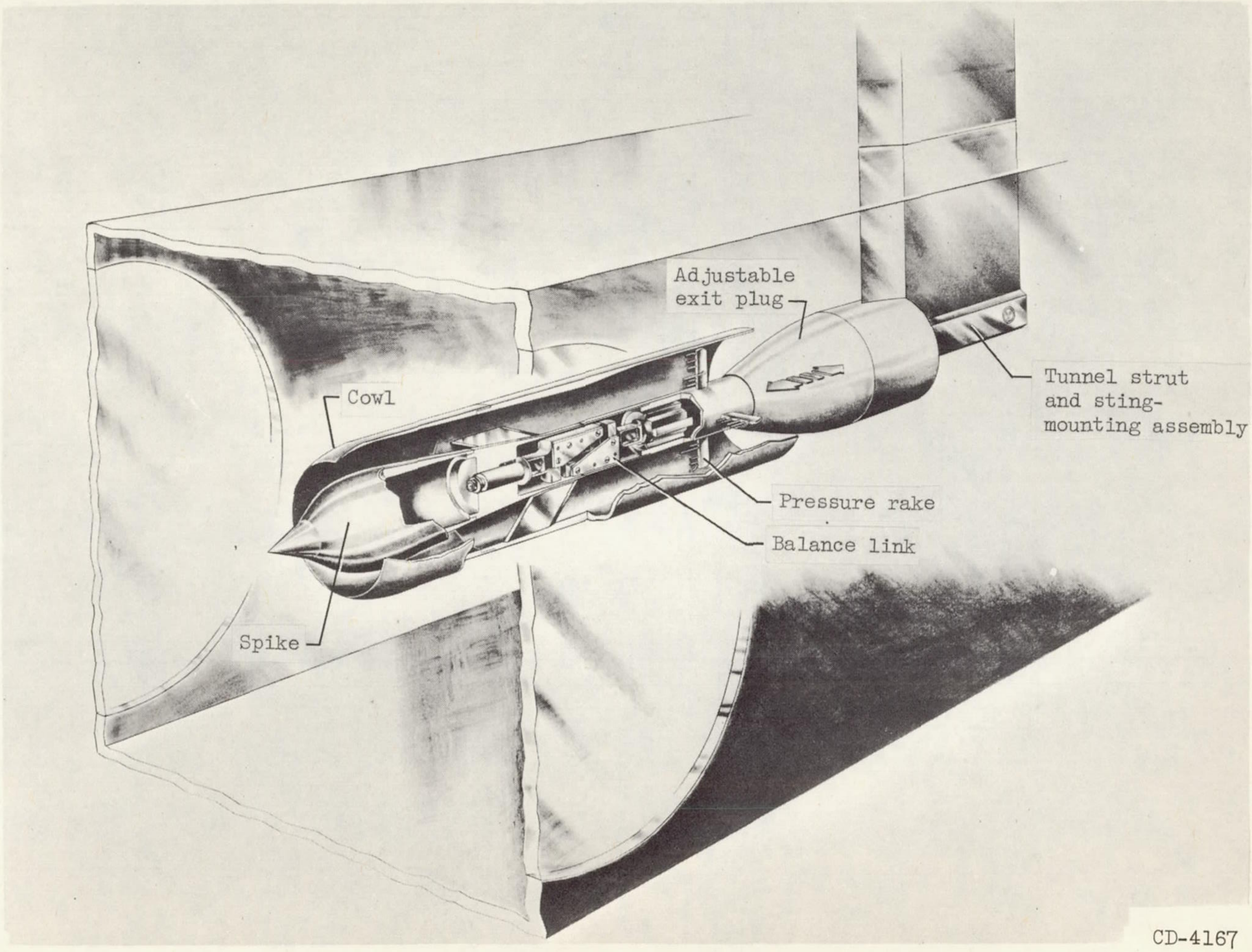

CD-4167

(a) 5-Inch-diameter model installation in 18- by 18-inch wind tunnel.

Figure 1. - Experimental models.

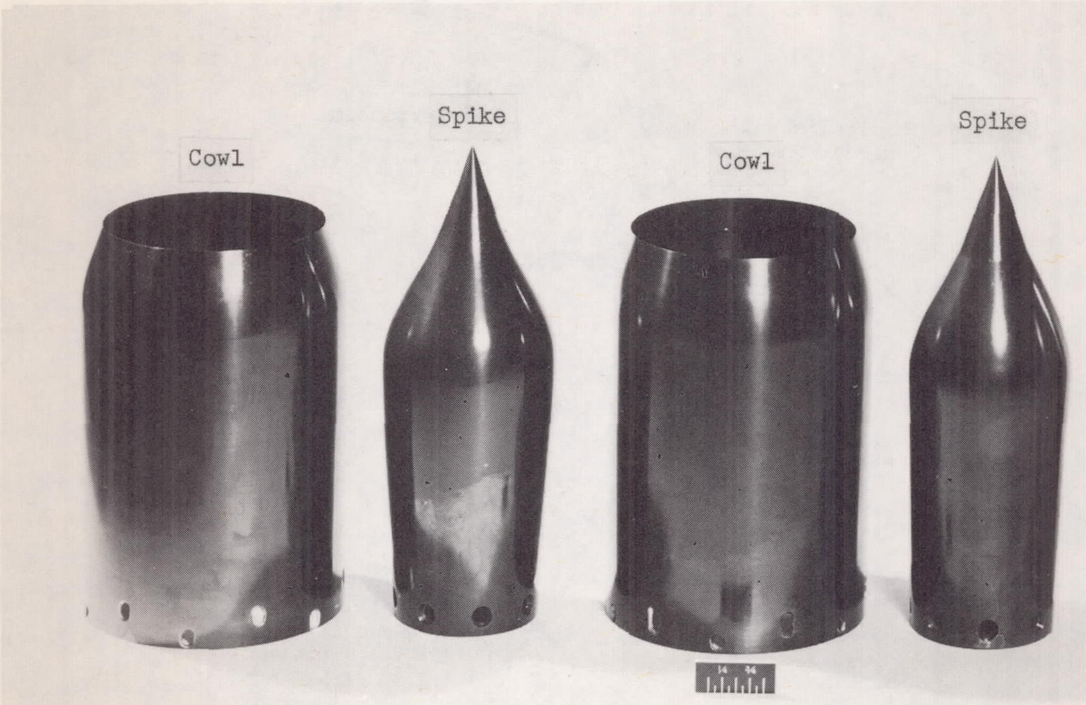

Isentropic inlet   Two-cone inlet   C-37399

(b) Inlet cowls and spikes.

Figure 1. - Continued. Experimental models.

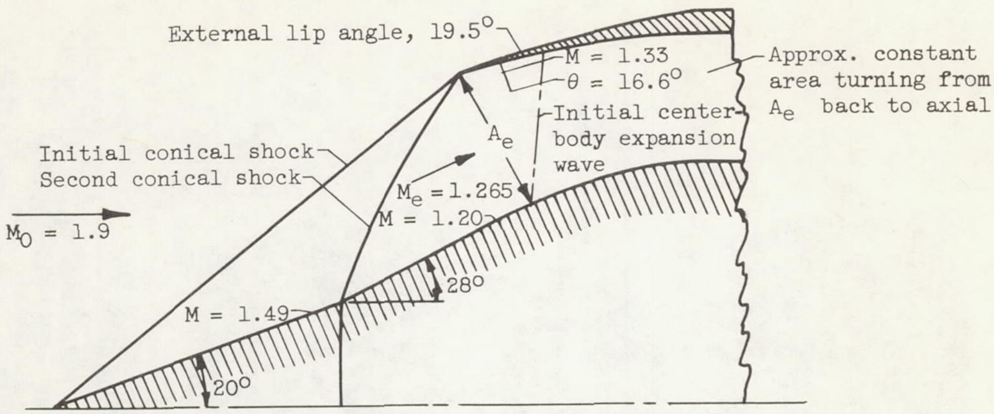

Two-cone inlet design

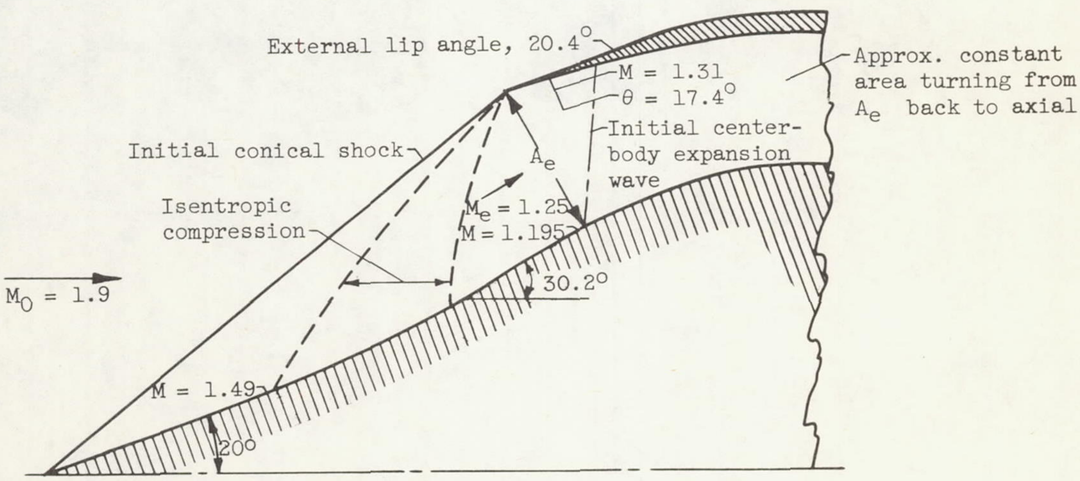

Isentropic inlet design

(c) Pertinent inlet design details.

Figure 1. - Continued. Experimental models.

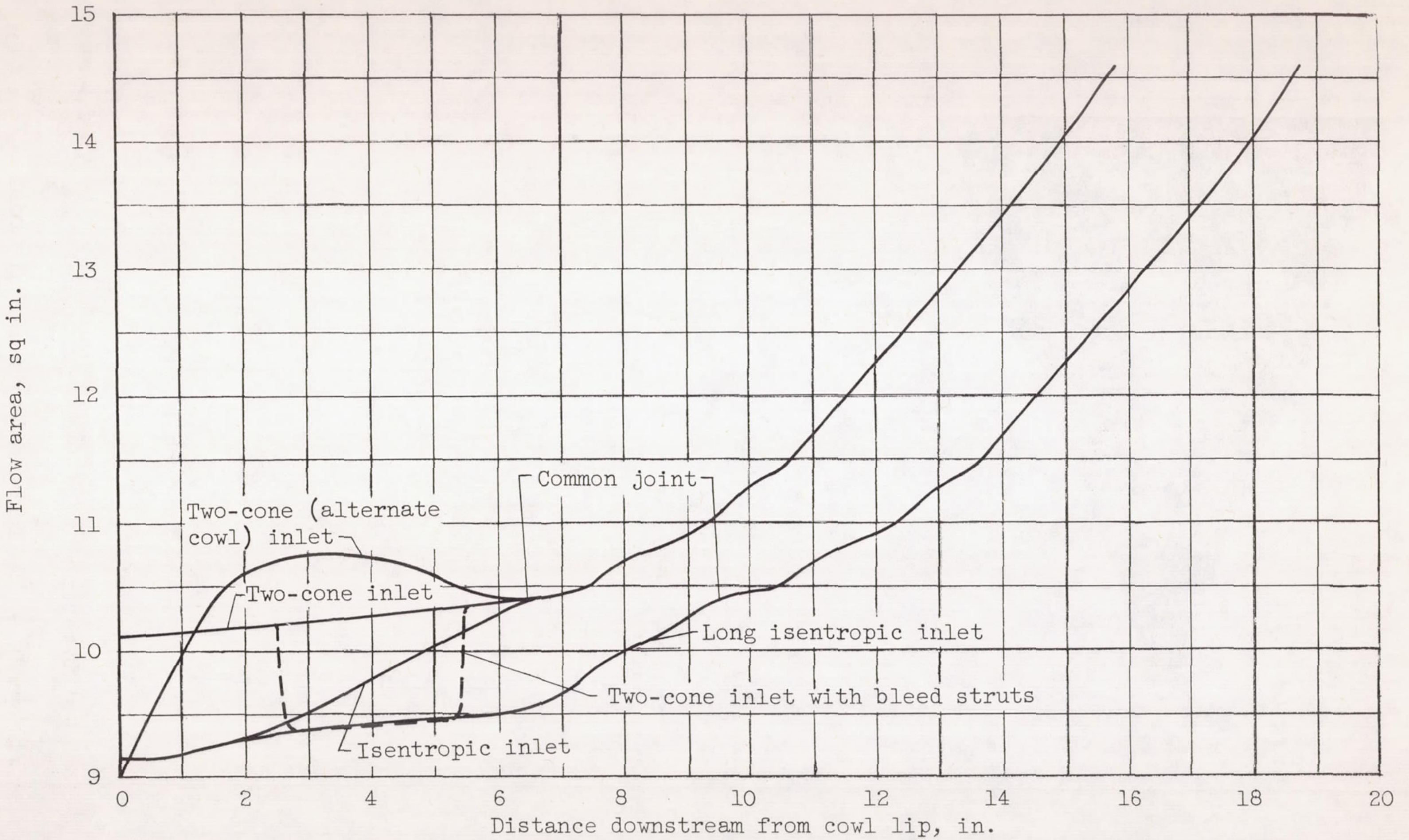

(d) Area distribution throughout various subsonic diffusers.

Figure 1. - Continued. Experimental models.

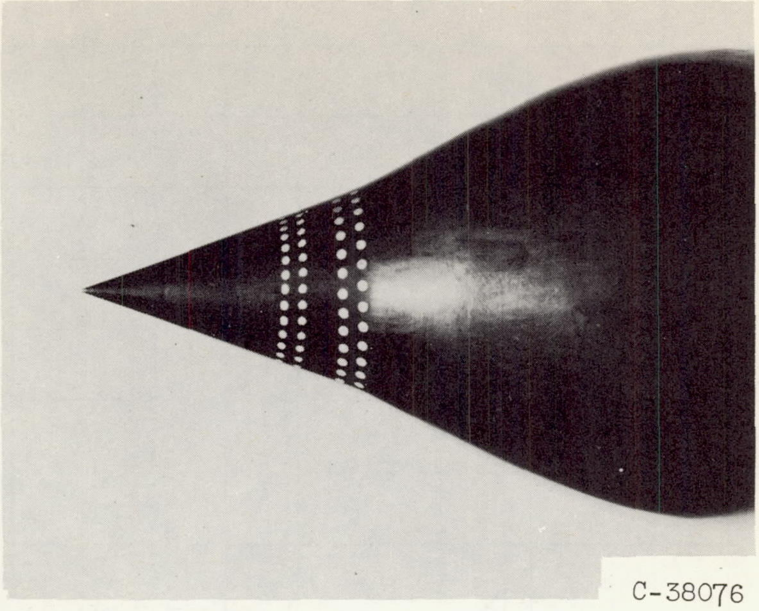

Perforated spike

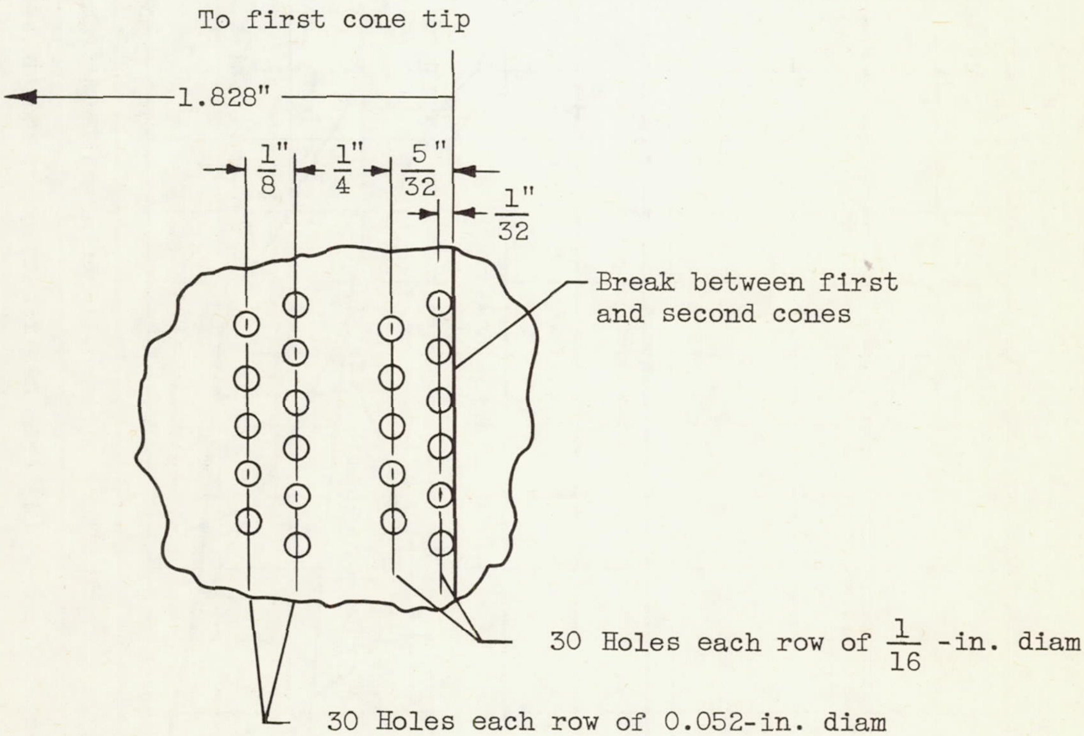

Hole pattern

(e) Two-cone spike perforation details.

Figure 1. - Concluded. Experimental models.

3706

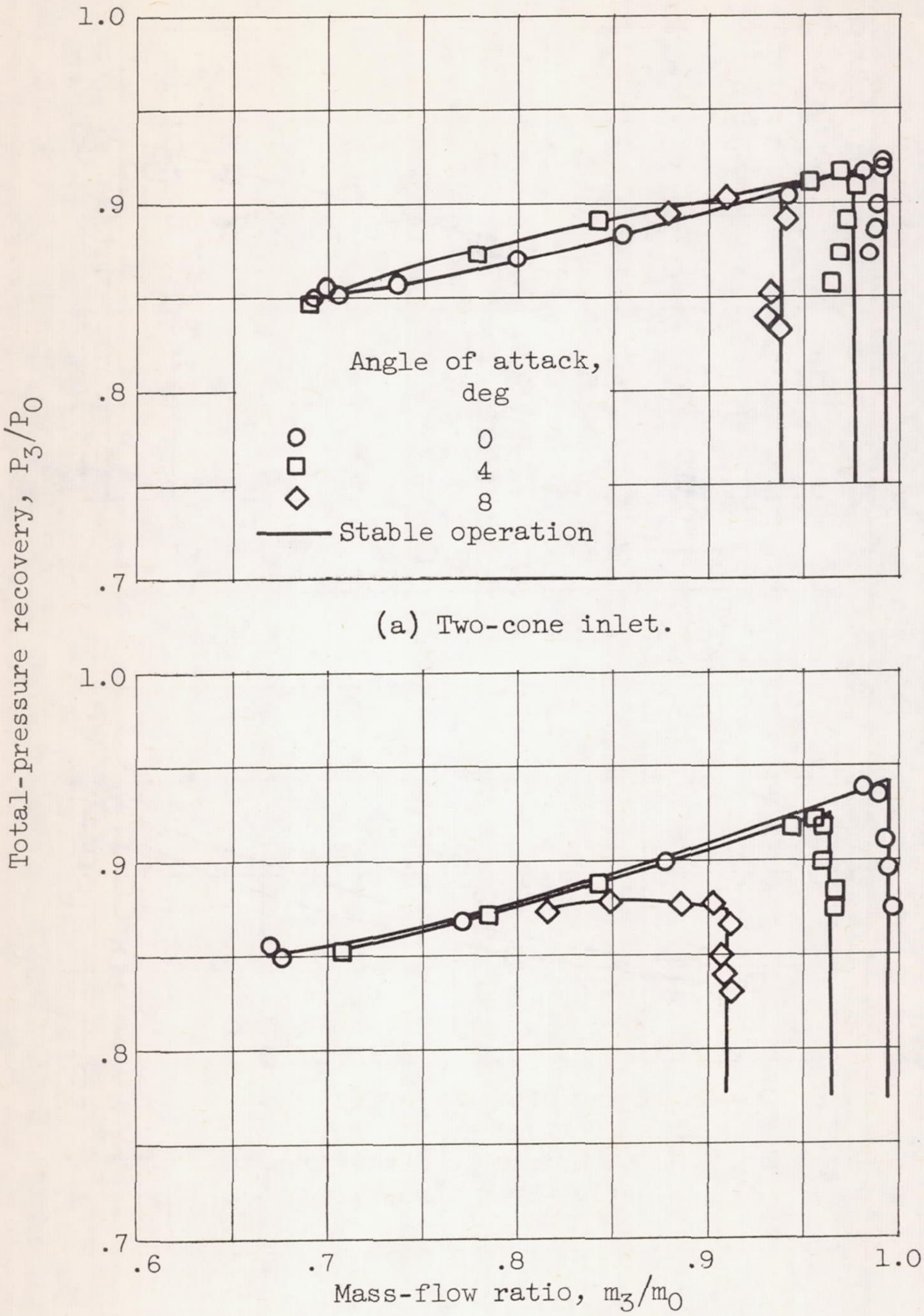

(a) Two-cone inlet.

(b) Isentropic inlet.

Figure 2. - Performance characteristics of axisymmetric two-cone and isentropic inlets at Mach number 1.9.

3706

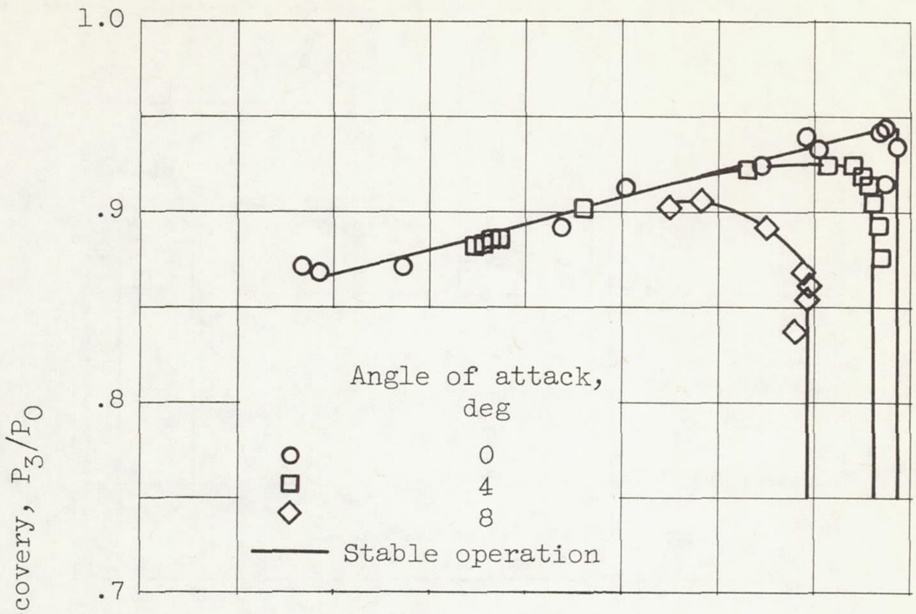

(c) Two-cone (alternate cowl) inlet.

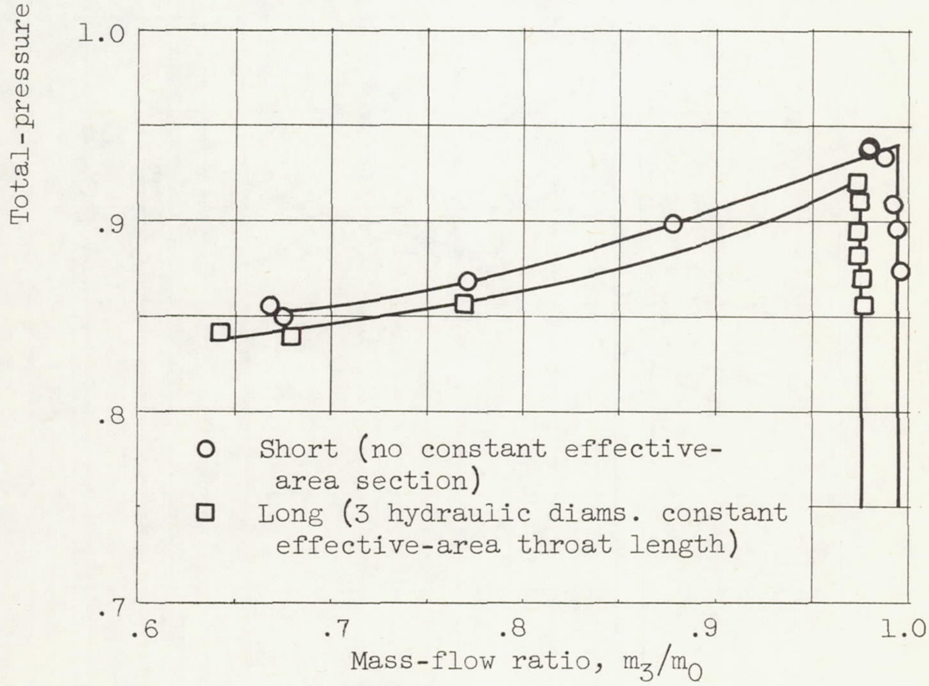

(d) Isentropic inlet.

Figure 2. - Continued. Performance characteristics of axisymmetric two-cone and isentropic inlets at Mach number 1.9.

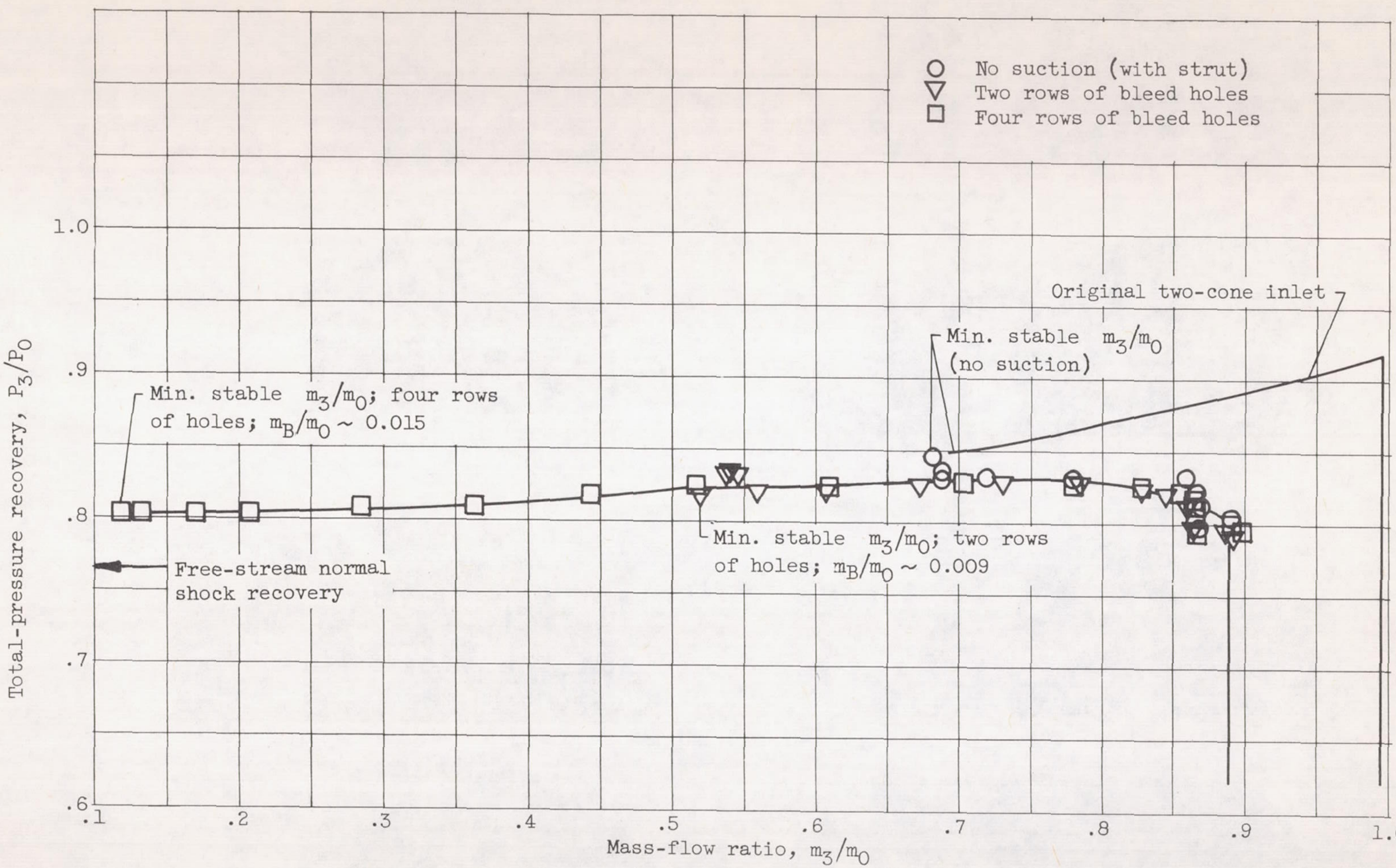

(e) Two-cone inlet with boundary-layer control; angle of attack, zero.

Figure 2. - Concluded. Performance characteristics of axisymmetric two-cone and isentropic inlets at Mach number 1.9.

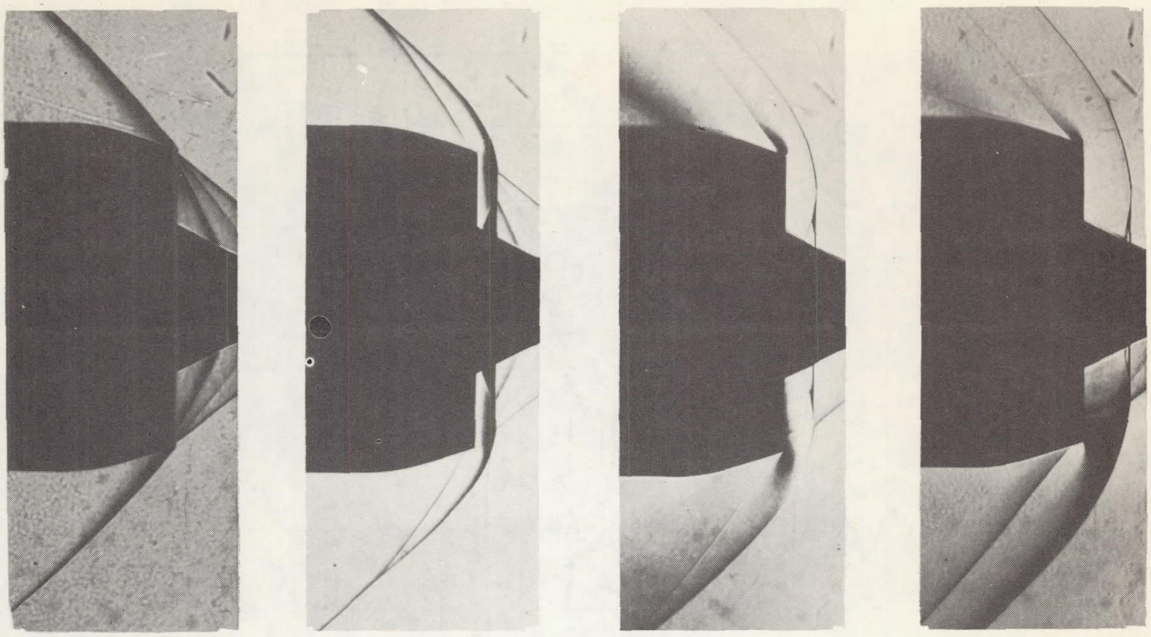

m_3/m_0 = 0.995; supercritical

m_3/m_0 = 0.855; subcritical

m_3/m_0 = 0.80; subcritical

m_3/m_0 = 0.695; min. stable

Angle of attack, zero

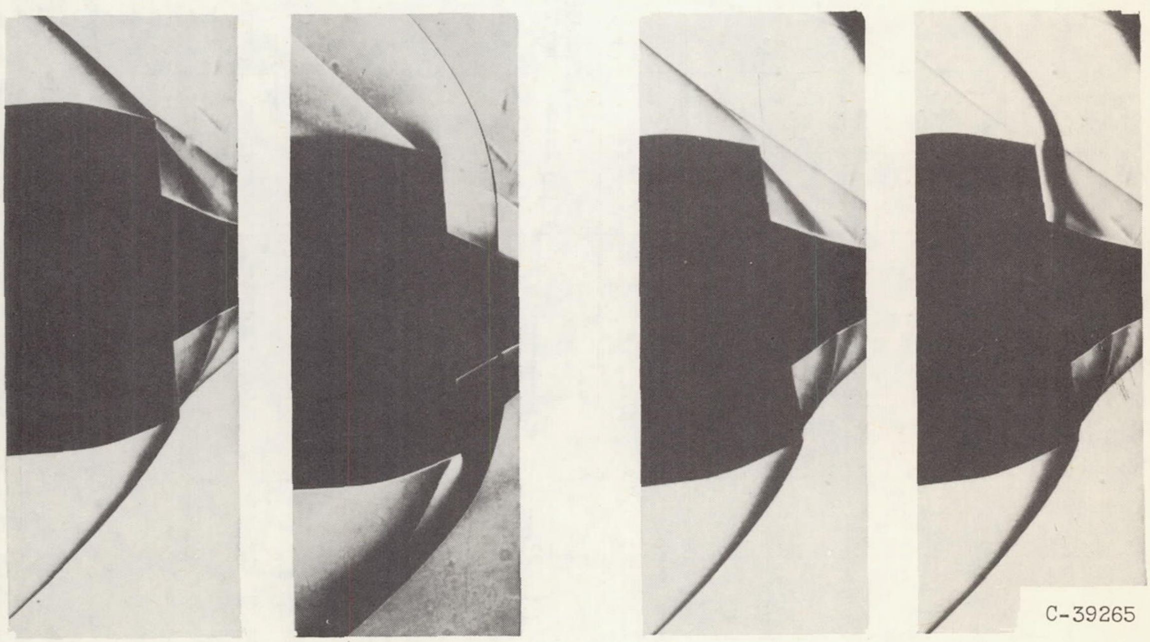

m_3/m_0 = 0.98; supercritical

m_3/m_0 = 0.69; min. stable

Angle of attack, 4°

m_3/m_0 = 0.94; supercritical

m_3/m_0 = 0.88; min. stable

Angle of attack, 8°

(a) Two-cone inlet.

Figure 3. - Inlet air-flow patterns.

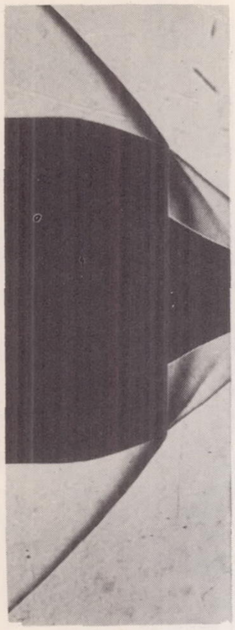

m_3/m_0 = 0.995;
supercritical

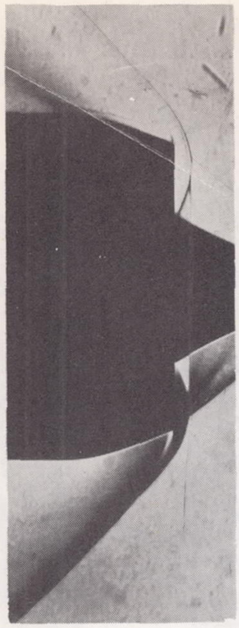

m_3/m_0 = 0.875;
subcritical

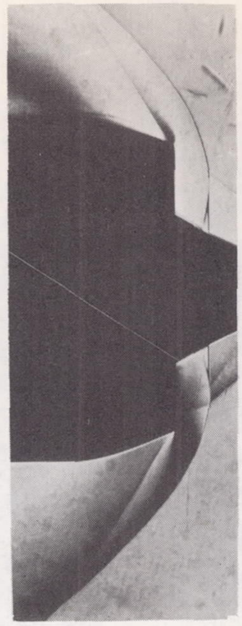

m_3/m_0 = 0.77;
subcritical

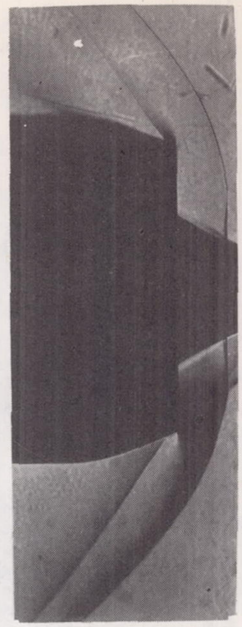

m_3/m_0 = 0.67;
min. stable

Angle of attack, zero

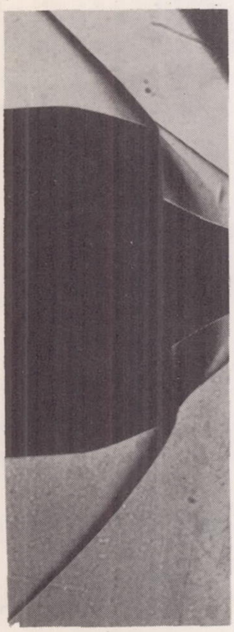

m_3/m_0 = 0.965;
supercritical

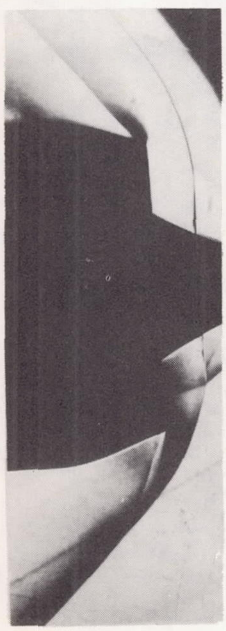

m_3/m_0 = 0.71;
min. stable

Angle of attack, 4°

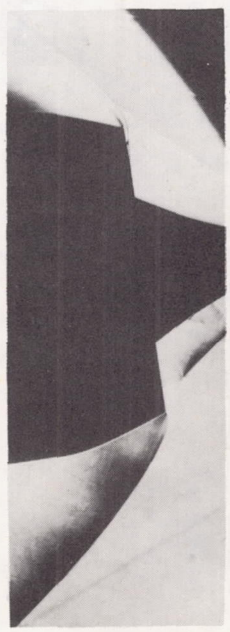

m_3/m_0 = 0.91;
supercritical

m_3/m_0 = 0.815;
min. stable

Angle of attack, 8°

(b) Isentropic inlet.

Figure 3. - Continued. Inlet air-flow patterns.

3706

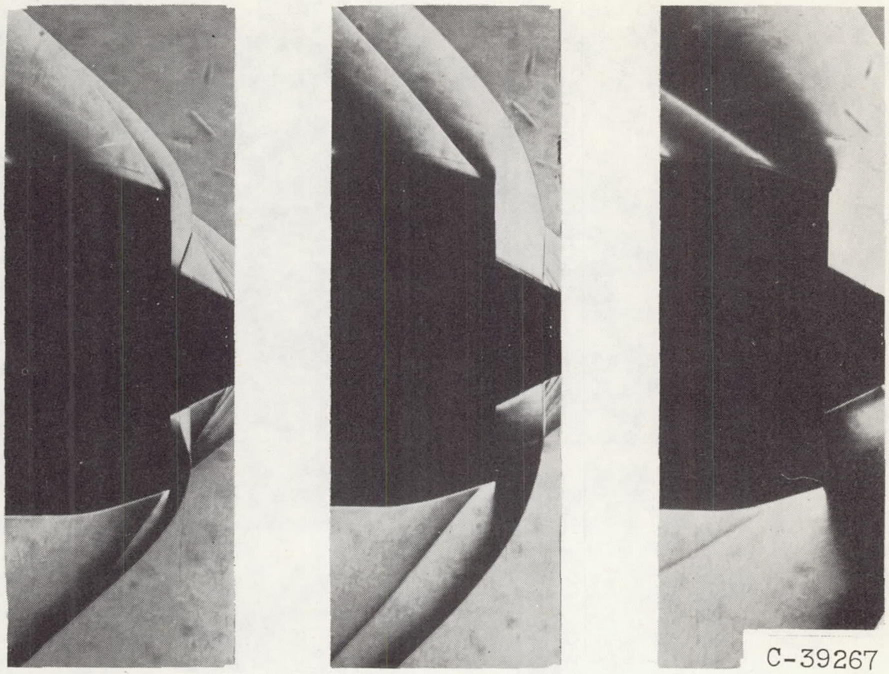

$m_3/m_0 = 0.89$; supercritical | $m_3/m_0 = 0.70$; subcritical | $m_3/m_0 = 0.12$; min. stable

(c) Two-cone (with boundary-layer suction) inlet. Angle of attack, zero.

Figure 3. - Concluded. Inlet air-flow patterns.

3706

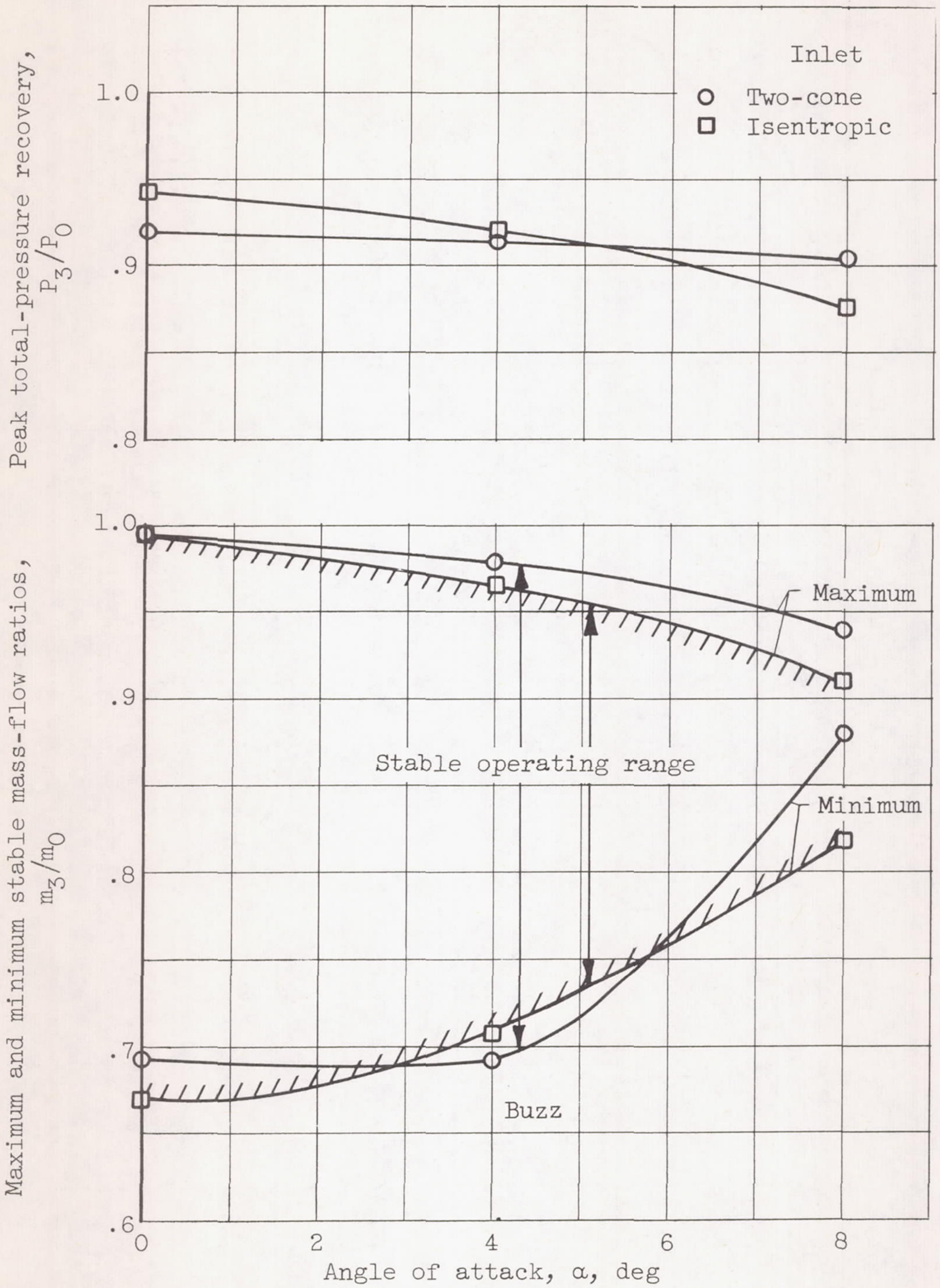

Figure 4. - Effect of angle of attack on performance of two-cone and isentropic inlets.

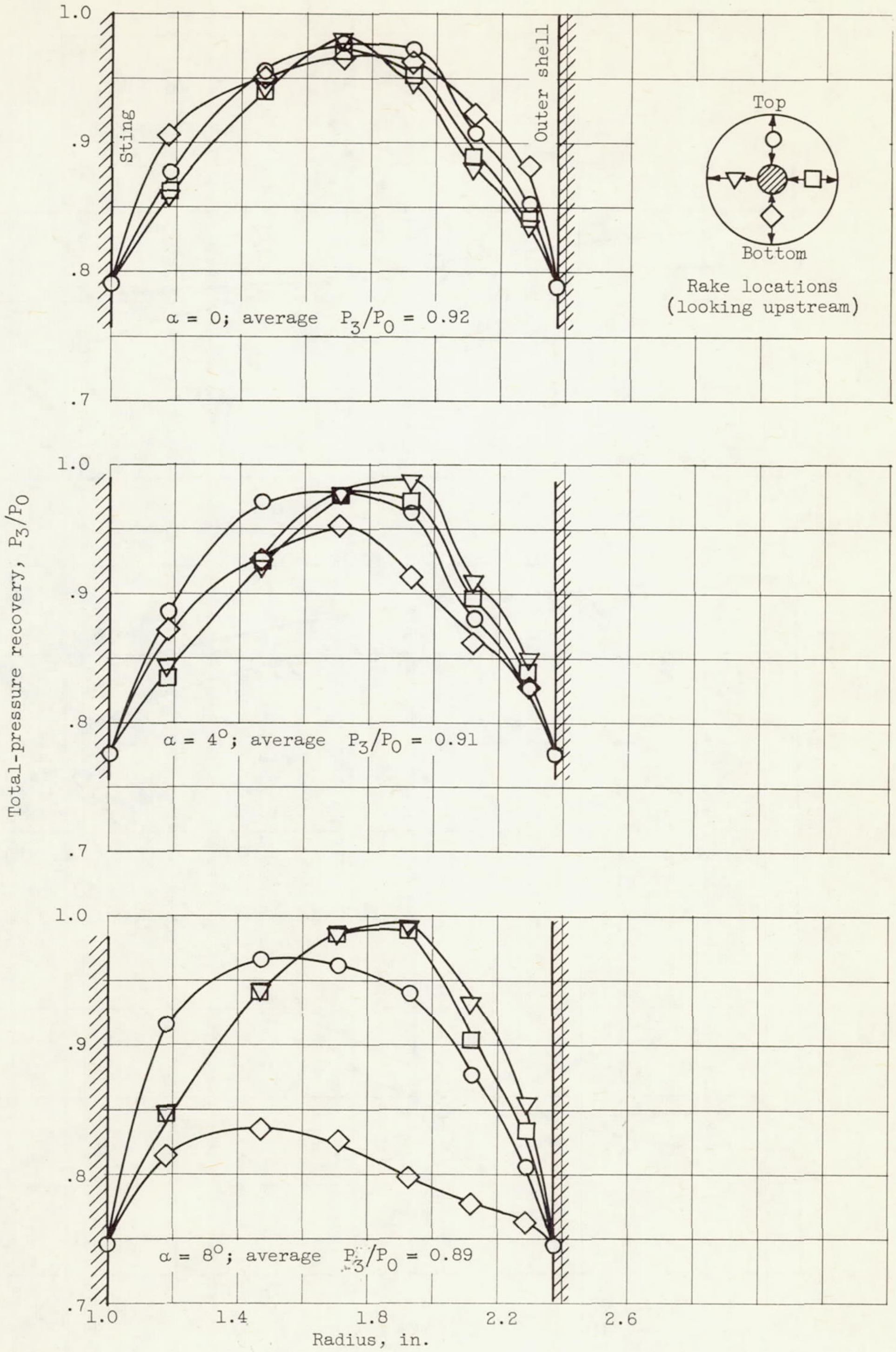

(a) Two-cone inlet.

Figure 5. - Total-pressure profiles at diffuser exit (near critical operation).

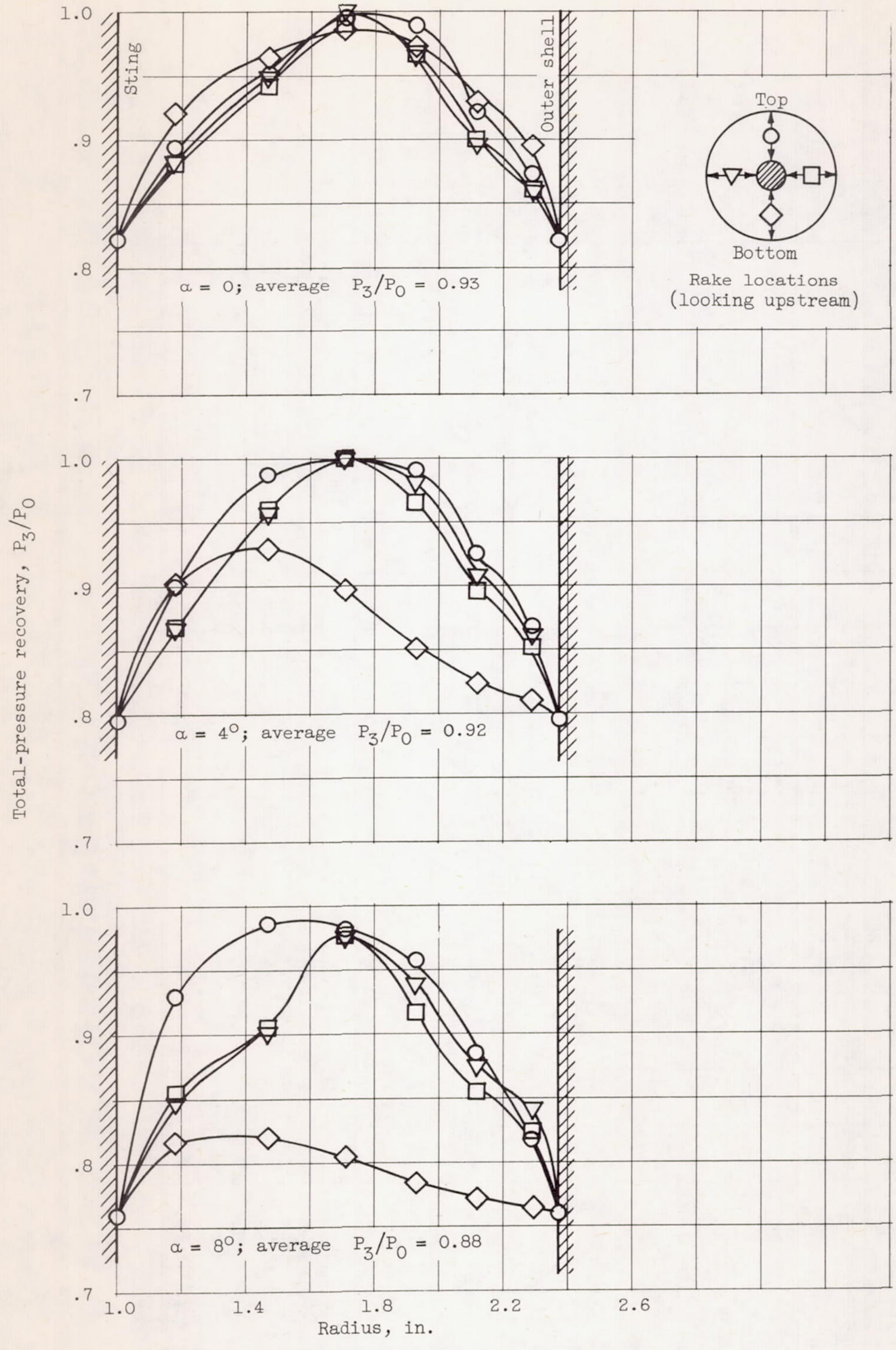

(b) Isentropic inlet.

Figure 5. - Concluded. Total-pressure profiles at diffuser exit (near critical operation).

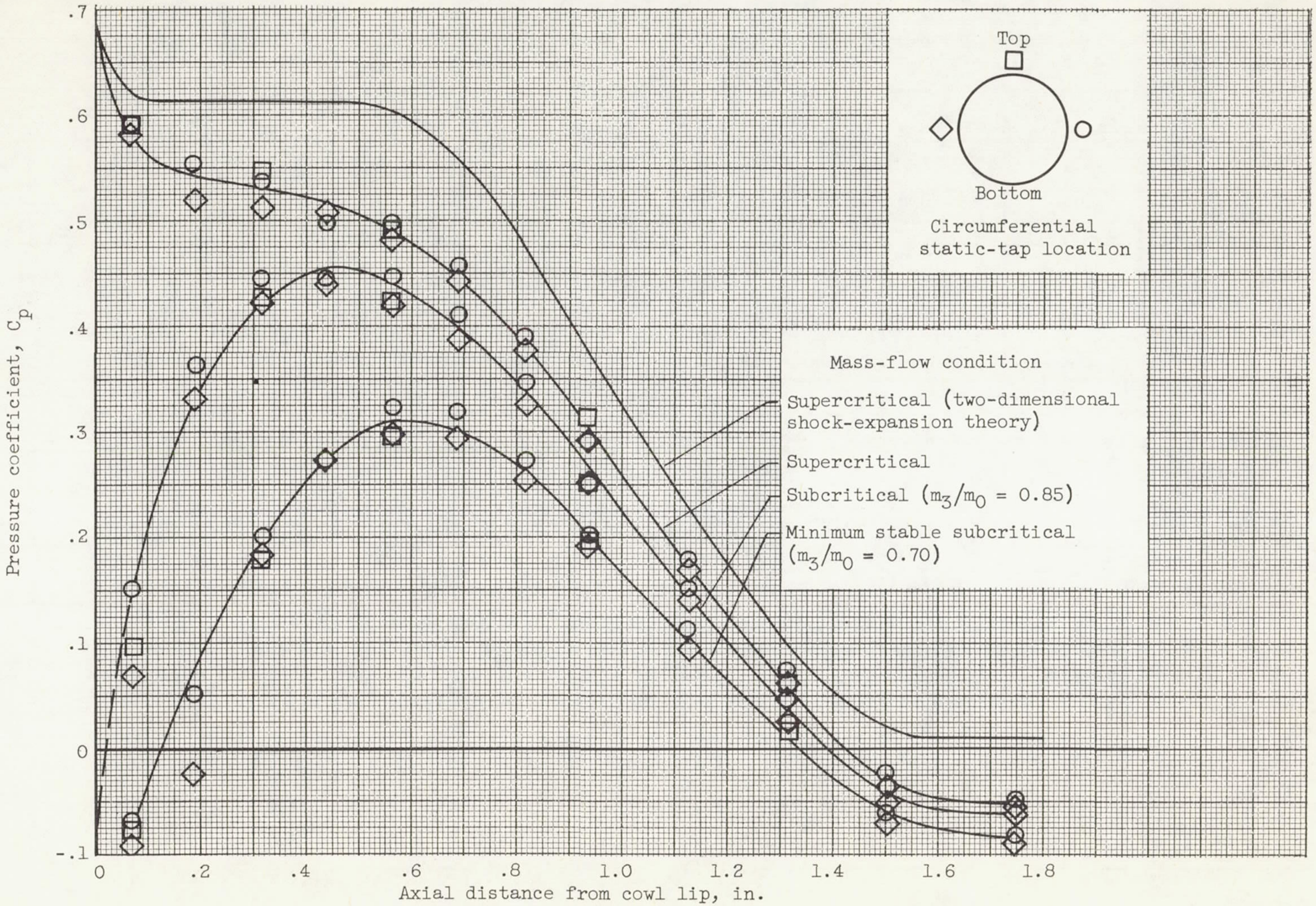

(a) Two-cone inlet.

Figure 6. - Cowl static-pressure distributions.

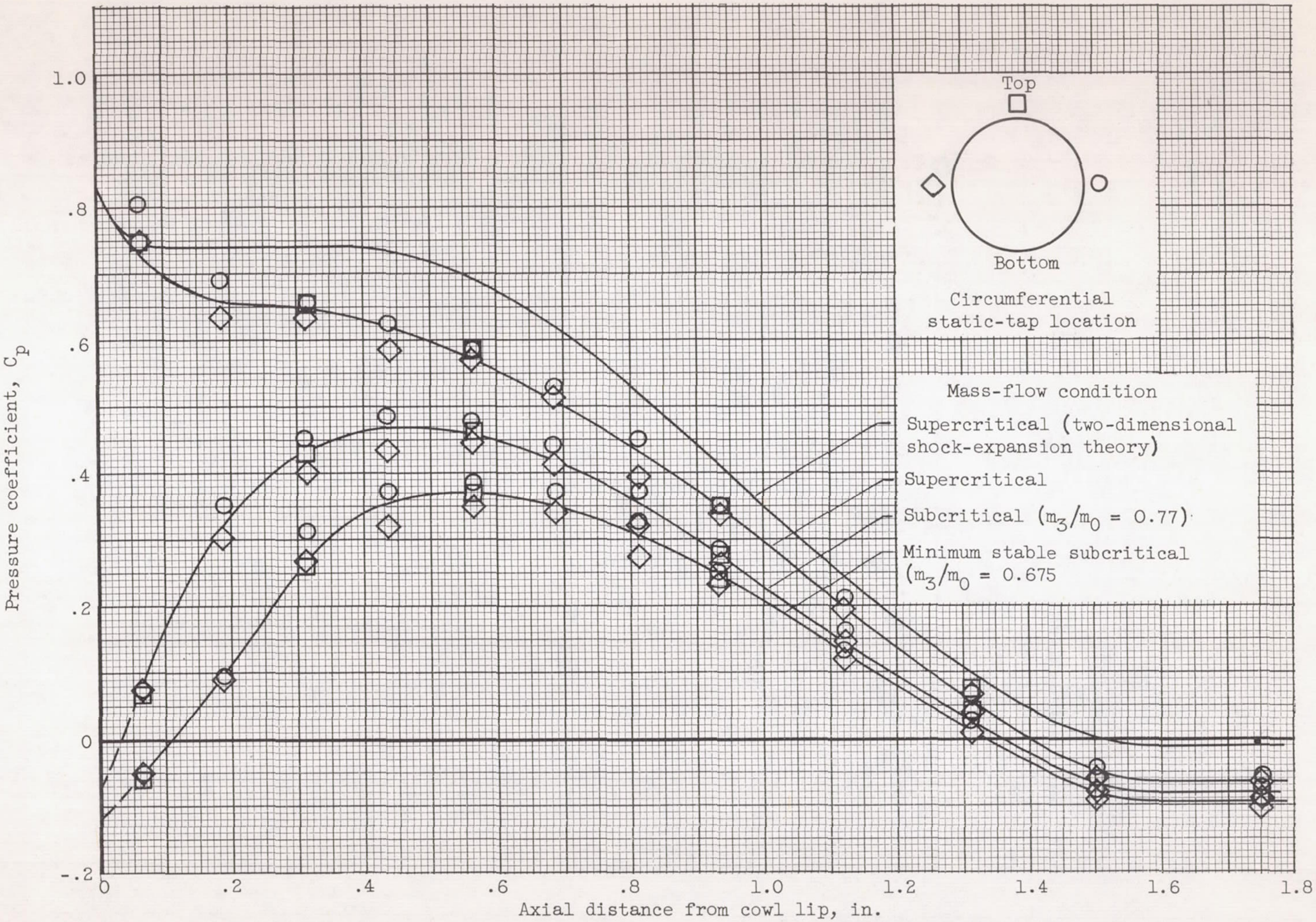

(b) Isentropic inlet.

Figure 6. - Concluded. Cowl static-pressure distributions.

3706

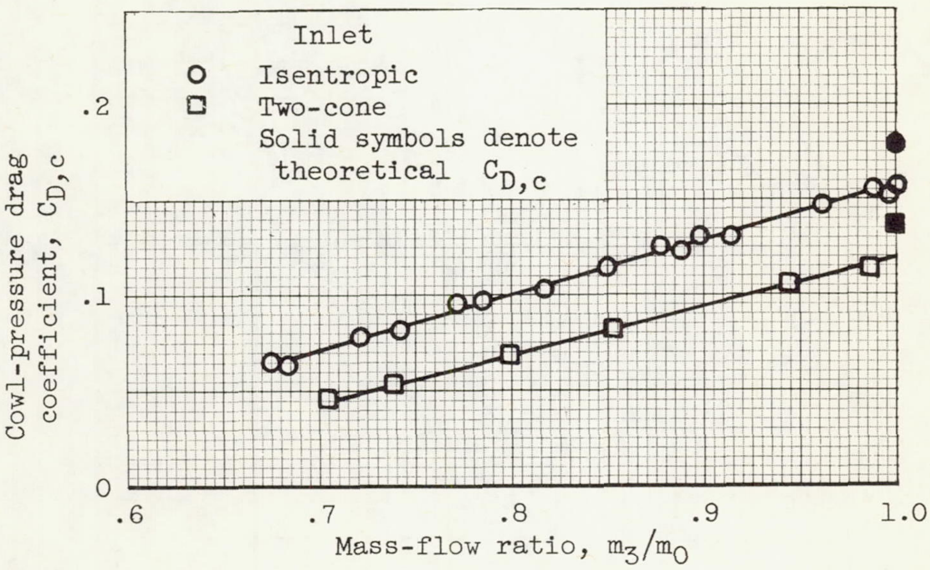

Figure 7. - Effect of spillage on cowl-pressure drag.

3706

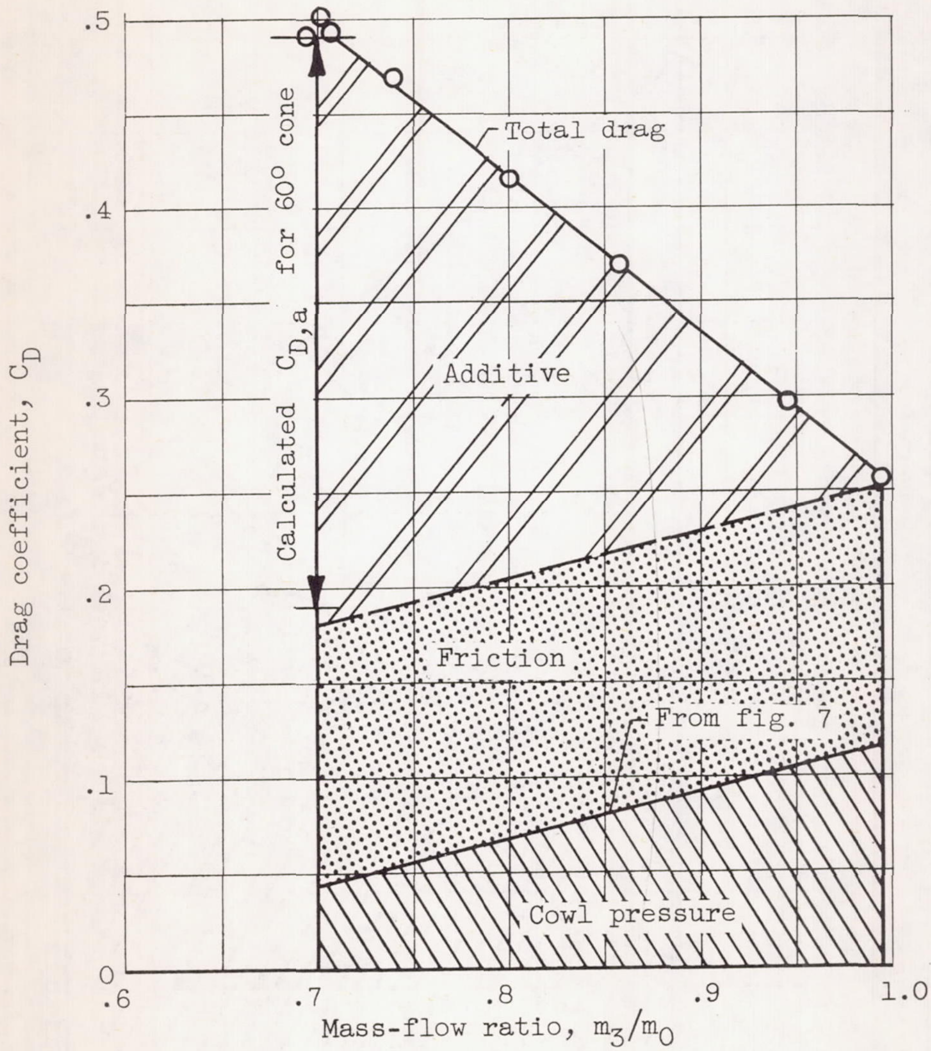

(a) Two-cone inlet.

Figure 8. - Component breakdown of external drag at zero angle of attack.

3706

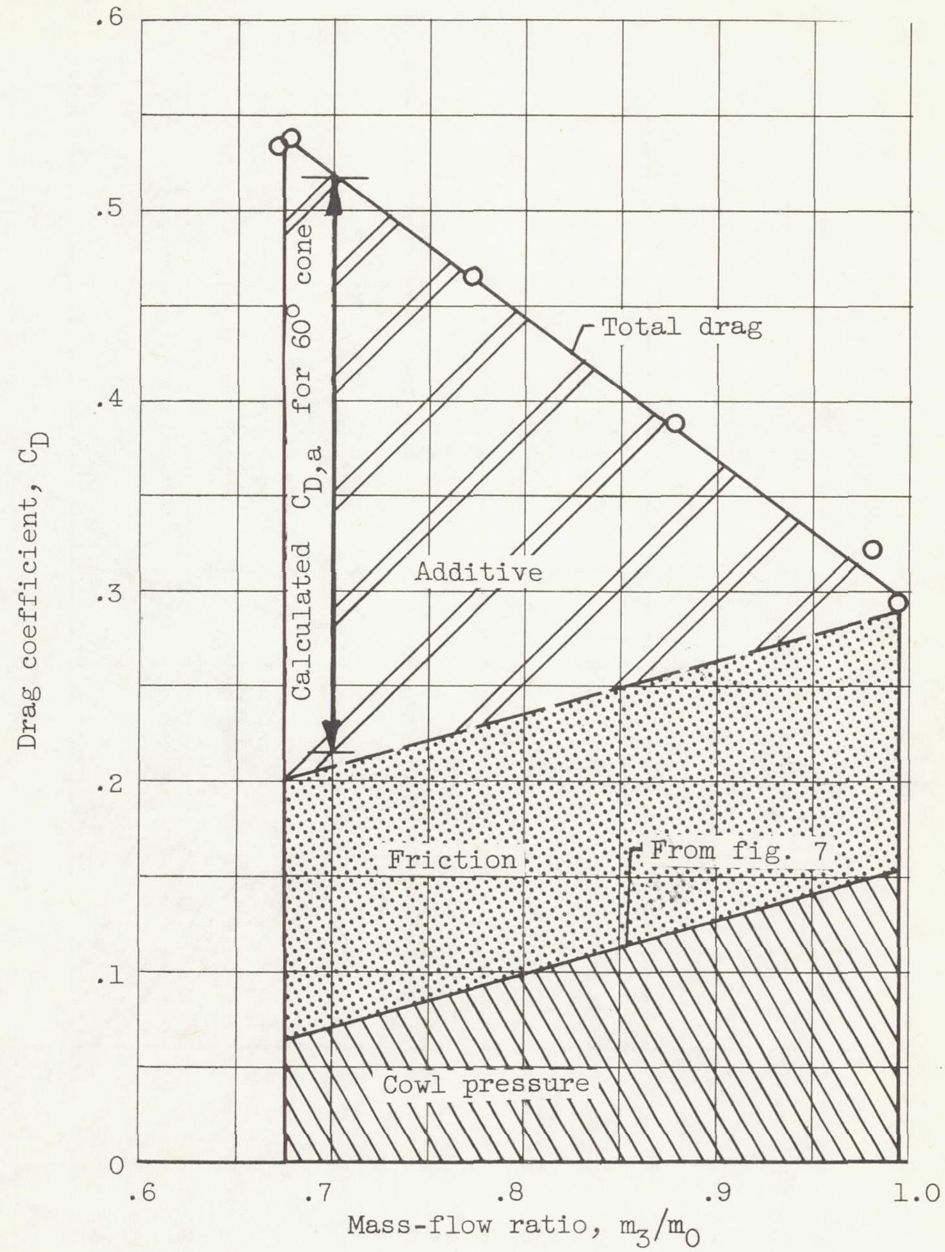

(b) Isentropic inlet.

Figure 8. - Concluded. Component breakdown of external drag at zero angle of attack.